DLINE JOURNALS

Journal of Digital Information Management

ISSN: 0972-7272

JDIM 2025: 23 (4)

Analyzing Outage Performance in a UAV-Assisted Backscatter System Operating under Realistic Composite Fading Conditions

Lam Dong Huynh[1], Lam Thanh Tu[2], Tan N. Nguyen[2]
[1]Faculty of Electrical and Electronics Engineering, Ton Duc Thang University
Ho Chi Minh City, Vietnam
huynhlamdong.st@tdtu.edu.vn

[2]Advanced Intelligent Technology Research Group, Faculty of Electrical and Electronics Engineering, Ton Duc Thang University
Ho Chi Minh City, Vietnam
tulamthanh@tdtu.edu.vn, nguyennhattan@tdtu.edu.vn

ABSTRACT

This paper analyzes the performance of a UAV-enabled backscatter communication system for low power IoT networks. The system consists of a power beacon that wirelessly energizes an energy constrained source node, which then transmits data to a UAV-mounted backscatter relay; the UAV reflects the signal to a destination. A realistic composite fading model is adopted: Rician fading for UAV-involved links (source-to-UAV and UAV-to-destination) to account for dominant line of sight (LoS) components, and Rayleigh fading for the ground based power beacon to source link due to shadowing. The main contribution is the derivation of an exact closed form expression for the system's outage probability using the Meijer G-function, enabling efficient performance evaluation without extensive simulations. The analysis incorporates a time switching protocol where the source alternates between energy harvesting and data transmission. Numerical results validate the analytical model and reveal critical insights: outage performance improves significantly with higher Rician K-factors (indicating stronger LoS), and an optimal time switching ratio exists that minimizes outage by balancing energy harvesting and data transmission durations. Additionally, hardware parameters such as backscatter coefficient and energy conversion efficiency strongly influence system reliability. The study also highlights the trade off between target data rate and outage probability, showing that higher beacon transmit power supports higher data rates at fixed reliability levels. These findings provide practical guidance for designing efficient UAV-assisted backscatter IoT systems.

Subject Categories and Descriptors:
[I.2.9 Robotics]; *Autonomous vehicles*: **[C.2.1 Network Architecture and Design];** *Wireless communication*

General Terms: UAV, Internet of Things, Wireless Communication

Keywords: Unmanned Aerial Vehicle (UAV), Backscatter Communication, Internet of Things (IoT), Energy

Harvesting, Outage Probability

Received: 28 June 2025, Revised 26 July 2025, Accepted 2 September 2025

Review Metrics: Review Scale: 1-6, Review Score: 4.65, Inter-reviewer consistency: 81.2%

DOI: https://doi.org/10.6025/jdim/2025/23/4/234-246

1. Introduction

The progression toward sixth generation (6G) wireless networks is motivated by the aspiration for a globally interconnected community, where the Internet of Things (IoT) framework is pivotal. This framework envisions a future filled with extensive connectivity, involving billions of low power, energy limited devices seamlessly integrated to facilitate a wide range of applications, including smart farming, environmental monitoring, industrial automation, and intelligent transportation systems [1]. However, achieving this ambitious vision on a large scale poses two fundamental and interconnected challenges: maintaining the sustainable operation of these devices and ensuring reliable communication links, especially for nodes situated in remote, hard to reach, or complex radio environments. The constraints of battery operated devices, which include limited operational lifetimes, high replacement costs, and environmental concerns, necessitate a transition to more sustainable energy solutions like RF energy harvesting. At the same time, the reliability and security of data transmission are often jeopardised by adverse propagation effects, such as path loss, shadowing, and multipath fading, which are particularly pronounced in terrestrial networks. Thus, the challenge lies not only in powering these networks but also in securing them, a topic that has been examined in recent research regarding secrecy performance in beacon powered IoT networks [14]. To tackle these challenges, innovative technologies that facilitate both energy efficient operation and adaptable on demand network deployment have become essential.

In this regard, two pivotal technologies have emerged as up and coming solutions: Unmanned Aerial Vehicles (UAVs) and backscatter communications. UAVs, utilized as airborne communication platforms, provide unmatched flexibility and mobility for deployment. Their ability to establish robust line of sight (LoS) communication links by operating at elevated altitudes enables them to circumvent terrestrial obstacles, thereby alleviating issues related to shadowing and severe fading that affect ground-based systems [2], [3]. The increasing sophistication of UAV technology, evidenced by applications ranging from autonomous positioning for power line inspections [12], to advanced optical stabilisation utilising fuzzy-based environmental detection [13], highlights their reliability and readiness for complex communication tasks. This positions UAVs as ideal can didates for serving as mobile base stations, on demand relays, or aerial data collectors, creating a dynamic and resilient layer within future heterogeneous wireless networks. In addition, backscatter communication offers an ultra low power approach for wireless data transmission. Rather than generating their own carrier waves, which is an energy consuming process, backscatter devices convey information by modulating and reflecting existing ambient Radio Frequency (RF) signals. This passive or semi passive transmission method significantly lowers the energy consumption and hardware complexity of IoT nodes, enabling near perpetual, “near zero power” communication [11].

The synergistic combination of UAVs and backscatter communications has recently garnered substantial research interest, promising to leverage the advantages of both technologies. The existing body of literature

has examined this synergy from various angles. A considerable amount of research has focused on using UAVs as dedicated mobile RF sources, powering and interrogating terrestrial backscatter devices [5], [6]. These studies often consider optimising the UAV's position or power beamforming to maximise the power delivered to the ground nodes. Another important research direction is using UAVs as mobile collectors/relays in a back scatter network of sensors [7], [8], whose common goal is to improve the UAV's trajectory, reduce the time required for data gathering, or maximise information dissemination.

In addition, research scientists have developed ways to incorporate. Alto online homework help, other advanced communication methods to improve these ideas, and other advanced techniques of communication. For instance, Non-NOMA Schemes in UAV-relay [9], and backscatter systems [10]. This trend also transfers to other new technologies like Machine to Open System Architecture (ROSA).

2. System Model

2.1 System Model Description

We consider a Unmanned Aerial Vehicle (UAV) enabled backscatter communication system [16], as illustrated in fig.1. The system comprises four main components: a dedicated Power Beacon (i.e., P), a Source (i.e., S), a backscatter device (i.e., B) mounted on the UAV, and a Destination (i.e., D). The energy constrained Lam Dong Huynh et al. source node S performs radio frequency (RF) energy harvesting from the signal transmitted by the Power Beacon P. After accumulating sufficient energy, Suses this harvested energy to transmit its information signal s (*t*) to UAV. Instead of decoding this signal, B exploits it as a carrier to convey its own symbol c (*t*) by changing its impedance and reflecting its modulation information back to D. Destination node D is the final information recipient.

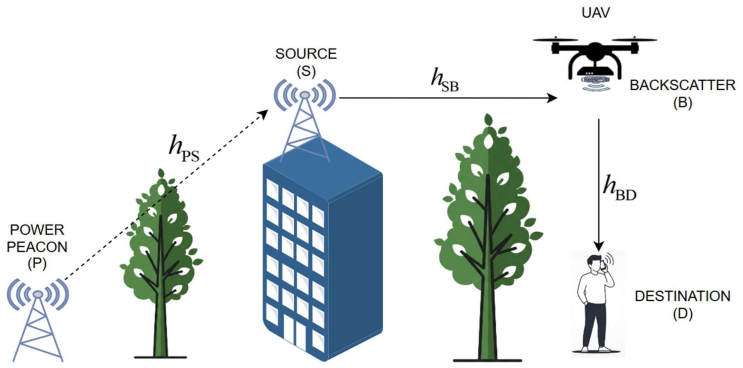

Figure 1. The system model of the UAV-assisted backscatter communication network

The wireless links in the network are modeled as follows:

• S-B and B-D Channels: Due to the high altitude of the UAV, it is likely that the links from source S to backscatter B (with channel gain h_{SB}) and from backscatter B to destination D (with channel gain hBD) have a Line of Sight (LoS) component. Therefore, we model these channels using Rician fading. The square of the channel gain amplitude, $|h_{SB}|^2 = \gamma_{SB}$ and $|hBD|^2 = \gamma_{BD}$ are Rician distributed random variables. The probability density function (PDF) of ³i can be given by [15]:

$$f_{\gamma_i}(x) = \frac{(K_i+1)e^{-K_i}}{\lambda_i} e^{-\frac{(K_i+1)x}{\lambda_i}} I_0\left(2\sqrt{\frac{K_i(K_i+1)x}{\lambda_i}}\right), \quad (1)$$

where i ε {SB,BD}, K is the Rician factor (the ratio of the power of the LoS component to the non-LoS components), λ_i is the mean value of γ_i, and I_o (.) is the zeroth order modified Bessel function of the first kind. Using the series expansion of $I_0(.), I_0(x) = \sum_{k=0}^{\infty} \frac{x^{2k}}{2^{2k}(k!)^2}$ the PDF can be rewritten as:

$$f_{\gamma_i}(x) = \zeta_i e^{-K_i} \sum_{k=0}^{\infty} \frac{(\zeta_i K_i)^k}{(k!)^2} x^k e^{-\zeta_i x}, \text{with} \zeta_i = \frac{K_i + 1}{\lambda_i} \quad (2)$$

The corresponding cumulative distribution function (CDF) of the RV γ_i can be derived as in [15] :

$$F_{\gamma_i}(x) = \int_0^x f_{\gamma_i}(t)dt = 1 - e^{-K_i} \sum_{l=0}^{\infty} \sum_{m=0}^{l} \frac{K_i^l \zeta_i^m}{l!m!} x^m e^{-\zeta_i x} \quad (3)$$

• *P-S* Channel: The link from the power beacon *P* to the source *S* (with channel gain hPS) is assumed to be heavily shadowed by ground obstacles. Consequently, this channel is modeled by Rayleigh fading. The square of the channel gain amplitude $|h_{PS}|^2 = \gamma_{PS}$ follows an exponential distribution with the PDF:

$$f_{\gamma_{PS}}(t) = \frac{e^{-\frac{t}{\lambda_{PS}}}}{\lambda_{PS}}, t \geq 0, \quad (4)$$

where γ_{PS} is the average value of γ_{PS}.

2.2 Energy Harvesting and Information Transfer Protocols

For energy harvesting and information processing, the time switching protocol is presented in fig.2. In this scheme, T is the block time in which the source fully transmits the information data to the destination. In addition, $\alpha T, \alpha \in [0,1]$ is the time in which the source harvests energy from the power beacon, and $(1-\alpha)T$ is used to transmit information to the destination. The communication protocol is divided into two phases:

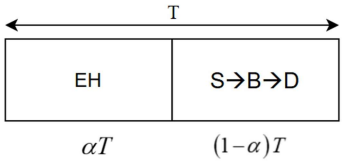

Figure 2. The energy harvesting and information processing in the system model

Energy Harvesting Phase:

During the first interval αT, the source node *S* switches to energy harvesting mode, accumulating energy from the RF signal transmitted by P. The energy harvested by the source *S* from *P* during the first phase is calculated as follows:

$$E_S = \eta \alpha T \gamma_{PS} P_P \quad (5)$$

where P_p is the transmit power of *P* and $\eta \in (0, 1)$ is the energy conversion efficiency.

The transmit power of *S* during the information transmission phase is:

$$P_S = \frac{E_S}{(1-\alpha)T} = \frac{\alpha\eta\, T P_P \gamma_{PS}}{(1-\alpha)T} = \kappa P_P \gamma_{PS} \quad (6)$$

with $\kappa = \frac{\alpha\eta}{1-\alpha}$

Information Transmission Phase:

In the remaining interval $(1-\alpha)T$, *S* utilizes the harvested energy to transmit its signal to the backscatter device *B*. Concurrently, *B* reflects this signal to *D* with it own message *c (t)* satisfying E {|c (t)|²}= 1. After being backscattered by *B*, the received signal at *D* [17], is derived by:

$$y_D = h_{SB} h_{BD} \sqrt{\beta P_S}\, s(t) c(t) + n_D = h_{SB} h_{BD} \sqrt{\beta \kappa P_P \gamma_{PS}}\, s(t) c(t) + n_D \quad (7)$$

where *s (t)* is the transmitted signal from *S*, in which E{|*s* (*t*)|²}= 1 and E{•} is the expectation operator; $0 < \beta \leq 1$ 1 is the backscatter coefficient of *B*, and n_D is the additive white Gaussian noise (AWGN) at *D* with variance No. Based on (7), the instantaneous signal to noise ratio (SNR) at *D* to detect the backscatter signal can be thus expressed as:

$$\gamma_D = \frac{\gamma_{SB}\gamma_{BD}\beta\kappa P_P \gamma_{PS}}{N_0} = \gamma_{SB}\gamma_{BD}\beta\kappa\Psi\gamma_{PS} \quad (8)$$

with $\Psi = \frac{P_P}{N_0}$

3. System Performance

In this section, we derive a closed-form analytical expression for the outage probability (OP) of the proposed UAV-assisted backscatter communication system. The OP is a key performance metric, defined as the probability that the instantaneous signal to noise ratio (SNR) at the destination D, γ_D , falls below a predefined threshold, γ_{th}.

The OP can be expressed as:

$$OP = \Pr(\gamma_D < \gamma_{th}) \quad (9)$$

By substituting the expression for (8) from the system model, we get:

$$OP = \Pr\left(\Psi\beta^2\kappa\gamma_{SB}\gamma_{BD}\gamma_{PS} < \gamma_{th}\right) = \Pr\left(\Phi\gamma_{PS} < \frac{\gamma_{th}}{\Psi\beta^2\kappa}\right) \quad (10)$$

where $\emptyset = \gamma SB\, \gamma BD$. For notational simplicity, we define .The OP can then be written as:

$$\mathrm{OP} = \Pr\left(\Phi < \frac{\xi}{\gamma_{PS}}\right) \quad (11)$$

To find the outage probability, we condition on the random variable γ_{PS} and integrate over its distribution. Since the *P-S* link follows Rayleigh fading, the channel power gain γ_{PS} is exponentially distributed with PDF as (4). The OP can be thus expressed as:

$$\mathrm{OP} = \int_0^\infty F_\Phi\left(\frac{\xi}{t}\right) f_{\gamma_{PS}}(t)\, dt \quad (12)$$

where $F_{\Phi}(\phi)$ is the cumulative distribution function (CDF) of the random variable = $\Phi = \gamma_{SB}\gamma_{BD}$. Since γ_{SB} and γ_{BD} are independent, the CDF of Φ can be derived as:

$$F_{\Phi}\left(\frac{\xi}{t}\right) = \Pr\left(\Phi < \frac{\xi}{t}\right) = \Pr\left(\gamma_{SB}\gamma_{BD} < \frac{\xi}{t}\right) = \Pr\left(\gamma_{SB} < \frac{\xi}{t\gamma_{BD}}\right) \\ = \int_0^{\infty} F_{\gamma_{SB}}\left(\frac{\xi}{ty}\right) f_{\gamma_{BD}}(y)\,dy \tag{13}$$

Based on (2), (3) the CDF of γ_{SB}, $F\gamma_{SB}(x)$, and the PDF of γ_{BD}, $f\gamma_{BD}(y)$, are given by

$$F_{\gamma_{SB}}(x) = \int_0^x f_{\gamma_{SB}}(t)dt = 1 - e^{-K_{SB}} \sum_{l=0}^{\infty}\sum_{m=0}^{l} \frac{K_{SB}^l \zeta_{SB}^m}{l!m!} x^m e^{-\zeta_{SB}x}, \text{ with} \zeta_{SB} = \frac{K_{SB}+1}{\lambda_{SB}} \tag{14}$$

$$f_{\gamma_{BD}}(y) = \zeta_{BD} e^{-K_{BD}} \sum_{k=0}^{\infty} \frac{(\zeta_{BD}K_{BD})^k}{(k!)^2} y^k e^{-\zeta_{BD}y}, \text{ with} \zeta_{BD} = \frac{K_{BD}+1}{\lambda_{BD}} \tag{15}$$

Substituting these into the expression for $F_{\Phi}\left(\frac{\xi}{t}\right)$ yields

$$F_{\Phi}\left(\frac{\xi}{t}\right) = \int_0^{+\infty}\left(1 - e^{-K_{SB}} \sum_{l=0}^{\infty}\sum_{m=0}^{l} \frac{K_{SB}^l \zeta_{SB}^m}{l!m!}\left(\frac{\xi}{ty}\right)^m e^{-\zeta_{SB}\frac{\xi}{ty}}\right) f_{\gamma_{SB}}(y)dy \\ = \int_0^{+\infty} f_{\gamma_{BD}}(y)dy - \int_0^{+\infty}\left(e^{-K_{SB}} \sum_{l=0}^{\infty}\sum_{m=0}^{l} \frac{K_{SB}^l \zeta_{SB}^m}{l!m!}\left(\frac{\xi}{ty}\right)^m e^{-\zeta_{SB}\frac{\xi}{ty}}\right) f_{\gamma_{BD}}(y)dy \\ = 1 - e^{-K_{SB}-K_{BD}}\zeta_{BD} \sum_{l=0}^{\infty}\sum_{k=0}^{\infty}\sum_{m=0}^{l} \frac{K_{SB}^l K_{BD}^k \zeta_{SB}^m \zeta_{BD}^k \left(\frac{\xi}{t}\right)^m}{l!m!(k!)^2} \int_0^{\infty} y^{(k-m)} e^{-\zeta_{SB}\frac{\xi}{ty} - \zeta_{BD}y} dy \tag{16}$$

The integral in the above expression can be solved using a standard identity from integral tables (e.g., Eq. 3.471.9 in [18]), which states

$$\int_0^{\infty} x^{y-1} e^{-\frac{\beta}{x} - \gamma x} dx = 2\left(\frac{\beta}{\gamma}\right)^{\nu/2} K_{\nu}\left(2\sqrt{\beta\gamma}\right) \tag{17}$$

where $K_{\upsilon}(.)$ is the modified Bessel function of the second kind of order υ. Setting $v = k - m + 1, \beta = \frac{\zeta_{SB}\xi}{t}, \gamma = \zeta_{BD}$, we obtain the closed form expression for $F_{\Phi}\left(\frac{\xi}{t}\right)$

$$F_{\Phi}\left(\frac{\xi}{t}\right) = 1 - 2e^{-K_{SB}-K_{BD}}\zeta_{BD} \\ \times \sum_{l=0}^{\infty}\sum_{k=0}^{\infty}\sum_{m=0}^{l} \frac{K_{SB}^l K_{BD}^k \zeta_{SB}^m \zeta_{BD}^k \left(\frac{\xi}{t}\right)^{\frac{m+k+1}{2}}}{l!m!(k!)^2} \left(\frac{\zeta_{SB}}{\zeta_{BD}}\right)^{\frac{k-m+1}{2}} K_{k-m+1}\left(2\sqrt{\zeta_{SB}\zeta_{BD}\frac{\xi}{t}}\right) \tag{18}$$

Now, we substitute (4) and (18) into the main outage probability formula.

$$
\begin{aligned}
\mathrm{OP} &= \int_0^{\infty} \left(\begin{array}{l} 1-2e^{-K_{\mathrm{SB}}-K_{\mathrm{BD}}\zeta_{\mathrm{BD}}} \\ \times \sum_{l=0}^{\infty}\sum_{k=0}^{\infty}\sum_{m=0}^{l} \frac{K_{\mathrm{SB}}^{l}K_{\mathrm{BD}}^{k}\zeta_{\mathrm{SB}}^{m}\zeta_{\mathrm{BD}}^{k}\left(\frac{\xi}{t}\right)^{\frac{m+k+1}{2}}}{l!m!(k!)^{2}} \left(\frac{\zeta_{\mathrm{SB}}}{\zeta_{\mathrm{BD}}}\right)^{\frac{k-m+1}{2}} K_{k-m+1}\left(2\sqrt{\zeta_{\mathrm{SB}}\zeta_{\mathrm{BD}}\frac{\xi}{t}}\right) \end{array} \right) \frac{e^{-\frac{t}{\lambda_{\mathrm{PS}}}}}{\lambda_{\mathrm{PS}}} dt \\
&= 1-2e^{-K_{\mathrm{SB}}-K_{\mathrm{BD}}\zeta_{\mathrm{BD}}} \sum_{l=0}^{\infty}\sum_{k=0}^{\infty}\sum_{m=0}^{l} \frac{K_{\mathrm{SB}}^{l}K_{\mathrm{BD}}^{k}\zeta_{\mathrm{SB}}^{m}\zeta_{\mathrm{BD}}^{k}}{l!m!(k!)^{2}} \left(\frac{\zeta_{\mathrm{SB}}}{\zeta_{\mathrm{BD}}}\right)^{\frac{k-m+1}{2}} \frac{\xi^{\frac{m+k+1}{2}}}{\lambda_{\mathrm{PS}}} \\
&\times \int_0^{\infty} t^{-\frac{m+k+1}{2}} e^{-\frac{t}{\lambda_{\mathrm{PS}}}} K_{k-m+1}\left(2\sqrt{\zeta_{\mathrm{SB}}\zeta_{\mathrm{BD}}\frac{\xi}{t}}\right) dt \\
&= 1-2e^{-K_{\mathrm{SB}}-K_{\mathrm{BD}}\zeta_{\mathrm{BD}}} \sum_{l=0}^{\infty}\sum_{k=0}^{\infty}\sum_{m=0}^{l} \frac{K_{\mathrm{SB}}^{l}K_{\mathrm{BD}}^{k}\zeta_{\mathrm{SB}}^{m}\zeta_{\mathrm{BD}}^{k}}{l!m!(k!)^{2}} \left(\frac{\zeta_{\mathrm{SB}}}{\zeta_{\mathrm{BD}}}\right)^{\frac{k-m+1}{2}} \frac{\xi^{\frac{m+k+1}{2}}}{\lambda_{\mathrm{PS}}} \Omega ,
\end{aligned}
\tag{19}
$$

Where

$$
\Omega = \int_0^{\infty} t^{-\frac{m+k+1}{2}} e^{-\frac{t}{\lambda_{\mathrm{PS}}}} K_{k-m+1}\left(2\sqrt{\frac{\zeta_{\mathrm{SB}}\zeta_{\mathrm{BD}}\xi}{t}}\right) dt \tag{20}
$$

By using the following formula as in [17], we have:

$$
K_{\nu}(x) = \frac{1}{2} G_{0,2}^{2,0}\left(\begin{array}{c} - \\ \frac{\nu}{2}, -\frac{\nu}{2} \end{array} \middle| \frac{x^2}{4} \right), \quad -\frac{\pi}{2} < \arg x \le \frac{\pi}{2} \tag{21}
$$

By substituting (21) into (20), Ω can be reformulated as:

$$
\Omega = \int_0^{\infty} t^{-\frac{m+k+1}{2}} e^{-\frac{t}{\lambda_{\mathrm{PS}}}} \frac{1}{2} G_{0,2}^{2,0}\left(\zeta_{\mathrm{SB}}\zeta_{\mathrm{BD}}\frac{\xi}{t} \middle| \begin{array}{c} - \\ \frac{k-m+1}{2}, -\frac{k-m+1}{2} \end{array}\right) dt \tag{22}
$$

Next, by applying the conversion formula: $G_{p,q}^{m,n}\left(\begin{array}{c} a_p \\ b_q \end{array} \middle| z \right) = G_{q,p}^{n,m}\left(\begin{array}{c} 1-b_q \\ 1-a_p \end{array} \middle| z^{-1} \right)$
Then, Ω can be re expressed by:

$$
\Omega = \int_0^{\infty} t^{-\frac{m+k+1}{2}} e^{-\frac{t}{\lambda_{\mathrm{PS}}}} \frac{1}{2} G_{2,0}^{0,2}\left(\frac{t}{\zeta_{SB}\zeta_{BD}\xi} \middle| \begin{array}{c} \frac{1-k+m}{2}, \frac{3+k-m}{2} \\ - \end{array}\right) dt \tag{23}
$$

With the help of equation 7.813.1 in [18], (23) can be found as

$$
\Omega = \frac{1}{2}\left(\frac{1}{\lambda_{\mathrm{PS}}}\right)^{\frac{m+k-1}{2}} G_{3,0}^{0,3}\left(\frac{\lambda_{\mathrm{PS}}}{\zeta_{\mathrm{SB}}\zeta_{\mathrm{BD}}\xi} \middle| \begin{array}{c} \frac{m+k+1}{2}, \frac{1-k+m}{2}, \frac{3+k-m}{2} \\ - \end{array}\right) \tag{24}
$$

Finally, by alternating (24) into (19), the OP of the proposed system is derived as follows

$$
\begin{aligned}
\mathrm{OP} &= 1-2e^{-K_{\mathrm{SB}}-K_{\mathrm{BD}}\zeta_{\mathrm{BD}}} \sum_{l=0}^{\infty}\sum_{k=0}^{\infty}\sum_{m=0}^{l} \frac{K_{\mathrm{SB}}^{l}K_{\mathrm{BD}}^{k}\zeta_{\mathrm{SB}}^{m}\zeta_{\mathrm{BD}}^{k}}{l!m!(k!)^{2}} \left(\frac{\zeta_{\mathrm{SB}}}{\zeta_{\mathrm{BD}}}\right)^{\frac{k-m+1}{2}} \xi^{\frac{m+k+1}{2}} \\
&\times \frac{\lambda_{\mathrm{PS}}^{-\frac{(m+k+1)}{2}}}{2} G_{3,0}^{0,3}\left(\frac{\lambda_{\mathrm{PS}}}{\zeta_{\mathrm{SB}}\zeta_{\mathrm{BD}}\xi} \middle| \begin{array}{c} \frac{m+k+1}{2}, \frac{1-k+m}{2}, \frac{3+k-m}{2} \\ - \end{array}\right)
\end{aligned}
\tag{25}
$$

This analytical result allows an efficient evaluation of the system outage performance under various channel conditions and system parameters. The accuracy of this derivation is validated against simulation results, as shown in the performance evaluation section.

4. Numerical Results and Discussion

λThis section presents a comprehensive numerical analysis to validate the derived analytical expressions and to offer deep insights into the performance of the proposed UAV-assisted backscatter communication system. We evaluate the outage probability (OP) under various system and channel conditions. Unless specified otherwise, the default simulation parameters are listed in Table 1. The infinite series in the analytical expressions are truncated at L_{max} = K_{max} = 20, which was confirmed to be sufficient for convergence.

Parameter	Description	Value
η	Energy conversion efficiency	0.8
β	Backscatter coefficient	0.5
α	Time-switching ratio	0.5
R	Target rate (bps/Hz)	0.5
υ	Path-loss exponent	2
d_{PS}, D_{SB}, D_{BD}	Distances (P-S, S-B, B-D)	1.5
KSB, KBD	Rician K-factors	5
λ_{PS}	Average channel power of P-S link	$d_{PS}^{-\upsilon}$
λ_{SB}, λ_{SD}	Average channel power of S-B, B-D links	$d_{SB}^{-\upsilon}$, $d_{BD}^{-\upsilon}$

Table 1. System Parameters and Their Values

4.1 Validation of Analytical Expressions

We begin by validating the accuracy of our derived closed form expression for the outage probability. Fig.3 plots the OP as a function of the normalized transmit power of the power beacon, $\Psi = \frac{P_P}{N_0}$. The analytical results (solid line) are juxtaposed with Monte Carlo simulations (circular markers). An excellent agreement between the two is observed across the entire range of transmit powers, which validates our analytical framework. The OP decreases monotonically with increasing, since a higher beacon power allows the source node S to harvest more energy, thereby increasing its transmit power and improving the end to end signal to noise ratio (SNR) at the destination D.

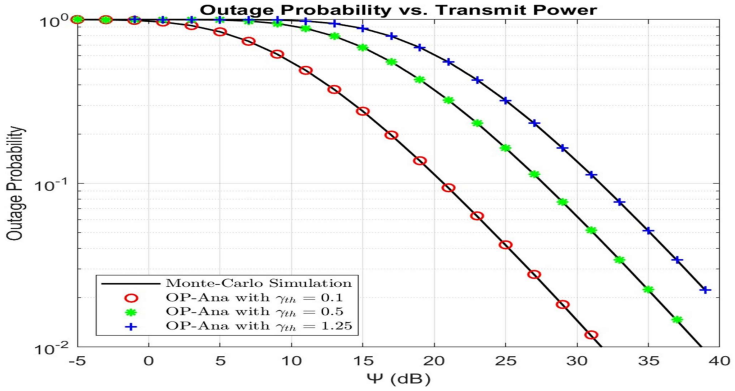

Figure 3. Outage Probability vs. Transmit Power of the Power Beacon, Ψ (dB).

4.2 Impact of Fading Channel Parameters

Next, we analyze the influence of the characteristics of the wireless channel on system performance. Fig.4 illustrates the effect of the Rician K-factor, which quantifies the strength of the Line of Sight (LoS) component. We assume symmetric UAV links ($K = K_{SB} = K_{BD}$). The results demonstrate that the system's performance is highly sensitive to the K-factor. A larger K-factor, signifying a more dominant LoS path, leads to a substantial improvement in outage performance. This is because a strong LoS component mitigates the severity of fading, resulting in a more reliable communication link. This finding underscores a principal advantage of deploying UAVs, which can often establish high quality LoS links by operating at altitudes that avoid terrestrial obstructions.

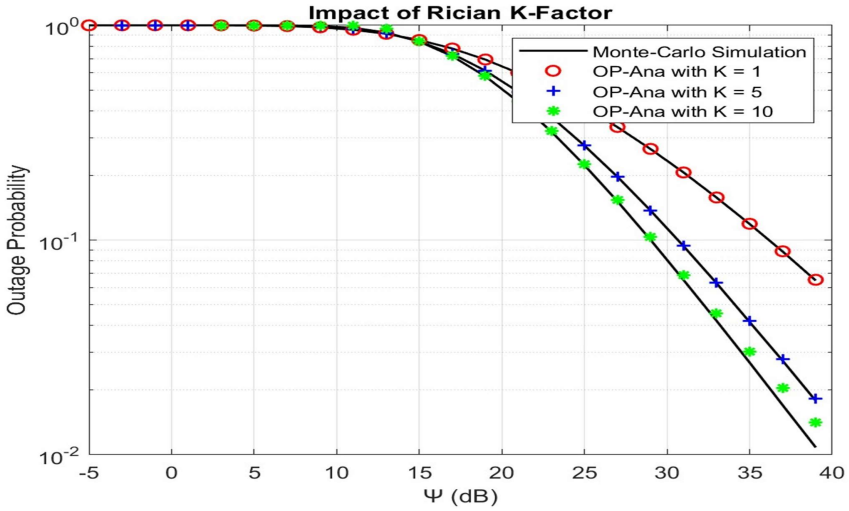

Figure 4. Outage Probability vs.Ψ(dB) for different Rician K-factors

4.3 Impact of Time Switching Protocol

The system performance is governed by key design parameters, which introduce fundamental trade offs. Fig.5 investigates the impact of the time switching ratio, α. This parameter partitions each time block T between energy harvesting (αT) and information transmission $(1-\alpha)T$. The convex shape of the curves indicates the existence of an optimal α that minimizes the outage probability. This trade off is fundamental: a small α allocates insufficient time for energy harvesting, leading to low transmit power PS, whereas a largeαleaves inadequate time for information transmission to meet the target rate R. It is also observed that the optimal value of α decreases as the available power from the beacon Ψ increases. When the beacon is powerful, the source can harvest sufficient energy in a shorter time interval, allowing more time to be allocated for data transmission.

4.4 Impact of Hardware Efficiency

Next, we explore the effect of hardware related parameters in Fig 6. The backscatter coefficient β determines the power reflection efficiency at the UAV, while the energy conversion efficiency η dictates how effectively the source converts received RF signals into usable DC power. The results show that the outage probability improves significantly with higher values of both β and η. While these are often fixed physical characteristics, this analysis quantifies their direct impact on system level performance. For instance, an improvement in back scatter efficiency from β= 0.6 to β = 0.8 can yield an order of magnitude reduction in outage probability in the high SNR regime, highlighting the critical importance of efficient component design for backscatter communication networks.

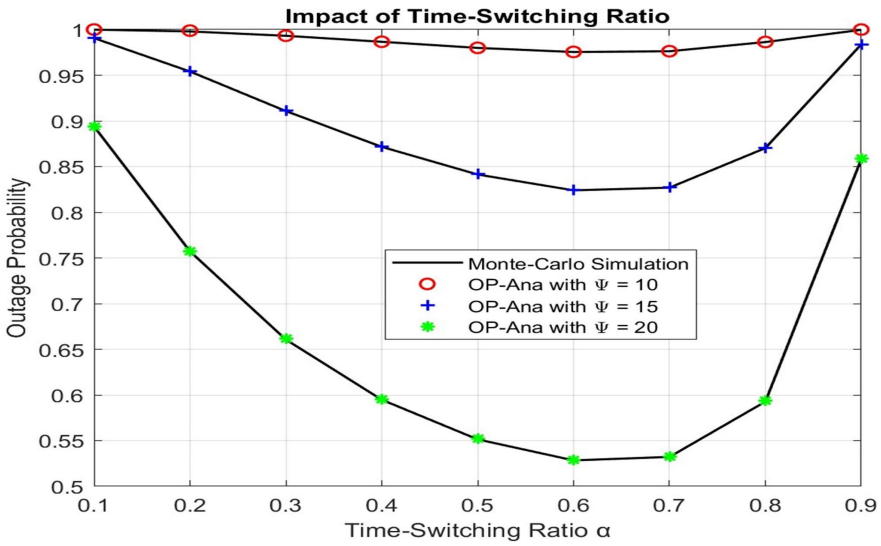

Figure 5. Outage Probability vs. Time Switching Ratio, for different values of Ψ

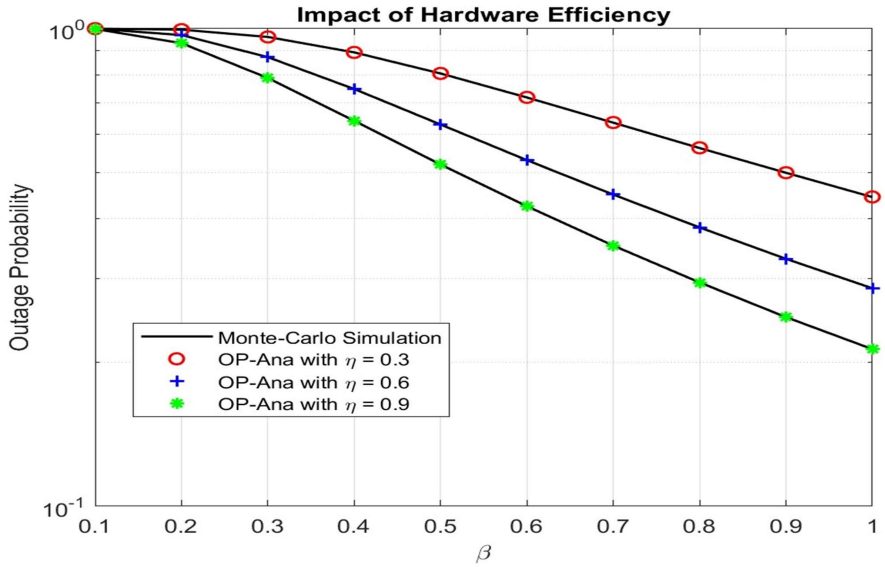

Figure 6. Outage Probability vsΨ (dB) for different values of backscatter coefficient (b) and energy conversion efficiency (h)

4.5 Impact of Target Data Rate

Finally, we investigate the impact of the target data rate, R, on the system's outage probability. The target rate is a fundamental quality of service (QoS) requirement, as it dictates the minimum spectral efficiency the system must achieve for successful communication. A higher target rate necessitates a higher SNR threshold, ³th, as defined by $\gamma_{th} = \frac{2R}{1-\alpha} - 1$. Consequently, for a fixed channel condition and transmit power, demanding a higher data rate makes the system more susceptible to outage events.

Fig.7 illustrates this trade-off by plotting the outage probability as a function of R for two fixed transmit power levels of the power beacon, $\Psi = 15dB$,$\Psi = 20dB$ and $\Psi = 25dB$. As expected, the outage probability increases monotonically with the target data rate for both power levels. This is because a higher R raises the required

SNR threshold, making it statistically less likely for the instantaneous end to end to exceed this threshold.

Furthermore, the figure quantifies the crucial role of the available power budget. By increasing the transmit power from $\Psi = 15dB$ to $\Psi = 20dB$ and then to $\Psi = 25dB$, the system can support a significantly higher data rate for the same outage probability. For instance, to maintain an outage probability of 10^{-1}, the system can support a rate of approximately 0.6 bit/s/Hz at Ψ = 15dB, whereas this rate increases to over 1.1 bit/s/Hz at Ψ = 25dB. This analysis highlights the inherent trade off between system reliability (outage probability) and spectral efficiency (data rate), and demonstrates how increased power can be leveraged to enhance the system's QoS capabilities.

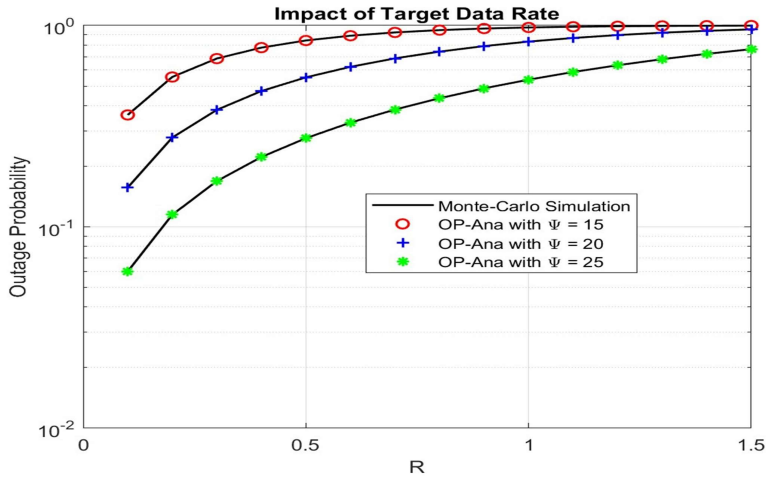

Figure 7. Outage Probability vs. Target Data Rate, R(bit/s/Hz), for different values of Psi

5. Conclusion

In this paper, we investigated the performance of a UAV-assisted backscatter communication system where an energy constrained source node is powered by a dedicated power beacon. We considered a comprehensive system model incorporating Rician fading for the UAV-to-ground and ground to UAV links, reflecting the likely presence of a Line of Sight component, and Rayleigh fading for the ground to ground link.

The primary contribution of this work is the derivation of a novel, exact closedform analytical expression for the system's outage probability. This expression, formulated using the Meijer G-function, provides an efficient tool for evaluating system performance without resorting to time consuming Monte Carlo simulations. Our numerical results have validated the accuracy of this analytical framework and offered several key insights. Specifically, we demonstrated that the system performance is highly dependent on the quality of the UAV links, with higher Rician K-factors leading to substantial improvements in outage probability. Furthermore, we analyzed the critical trade off in time allocation for energy harvesting versus information transmission, showing the existence of an optimal time switching ratio that minimizes the outage probability. The analysis also quantified the significant impact of hardware parameters, such as the backscatter coefficient and energy conversion efficiency, on the overall system performance.

For future work, this study can be extended in several promising directions. One interesting avenue is the optimization of the UAV's trajectory to further enhance system performance. Investigating resource allocation in a multi user scenario, where the UAV serves multiple backscatter devices, presents another challenging yet

practical problem. Finally, considering the impact of imperfect channel state information (CSI) or hardware impairments would provide a more complete understanding of the system's performance in practical deployment scenarios.

References

[1] Qadir, Z., Le, K., Saeed, N., Munawar, H. (2023). Towards 6G Internet of Things: Recent advances, use cases, and open challenges. *ICT Express* 9 (3), 296–312 https://doi.org/10.1016/j.icte.2022.06.006.

[2] Ho-Van, K., Do-Dac, T. (2021).Performance Analysis of Energy Harvesting UAV Selection. *Wireless Communications and Mobile Computing* (1), 5545910. https://doi.org/10.1155/2021/5545910.

[3] Bui Vu, M., Le, A. T., Le, C. B., Nguyen, S. Q., Phan, V. D., Nguyen, T. N., Voznak, M. (2023). Performance Predi ction in UAV-Terrestrial Networks With Hardware Noise. *IEEE Access* 11, 117562–117575 https://doi.org/10.1109/ACCESS.2023.3325478.

[4] Le, A. T., Nguyen, T. N., Tu, L. T., Tran, T. P., Duy, T. T., Voznak, M., Ding, Z. (2024). Performance Analysis of RIS-Assisted Ambient Backscatter Communication Systems. *IEEE Wireless Communications Letters* 13 (3), doi:10.1109/LWC.2023.3344113.

[5] Yang, G., Liang, Y. C., Zhang, R., Pei, Y. (2018). Modulation in the air: Backscatter communication for wireless-powered cognitive radio networks. *IEEE Transactions on Communications* 66 (3) 1219–1233 (2018). DOI:10.1109/TCOMM.2017.2772261.

[6] Park, H. S., Kim, S. H., Kim, D. I. (2020). UAV-aided backscatter communications for massive IoT networks. *IEEE Transactions on Wireless Communications* 19 (12) 8235–8248.

[7] Li, Z., Chen, M., Yang, Z., Han, Z. (2020). UAV-assisted data collection in backscatter sensor networks. *IEEE Transactions on Vehicular Technology* 69 (10) 12059–12072 .

[8] Tran, H. D. T., Koo, I. (2020). UAV-Enabled Wireless Powered Communication Networks: A Joint Trajectory and Resource Allocation Optimization. *Sensors* 20 (17) 4933.

[9] Bao, V. N. Q., Chien, T. V., Van, N. T. T., Voznak, M. (2021). Performance of UAVRelay Assisted NOMA Networks with Wireless Power Transfer. *Applied Sciences* 11 (15) 7001.

[10] Nguyen, D. C., Chaitanya, M. S. V. S. K., Nguyen, H.V., Nguyen, V. D. (2020). Performance Analysis of NOMA-Based Backscatter Communication Systems With Wireless Powering. *IEEE Access* 8, 62141–62153.

[11] Le, V., Nguyen, H., Nguyen, S., Bui, T., Hien, D., Kim, B. (2025). Enabling D2D transmission mode of reconfigurable intelligent surfaces aided in wireless NOMA system. Adv. *Electr. Electron. Eng*. 23 (1) 32–42 https://doi.org/10.15598/aeee.v23i1.240809.

[12] Voon, S., Kho, L., Ngu, S., Joseph, A., Kipli, K. (2024). Autonomous positioning of unmanned aerial vehicle (UAV) for power lines insulator detection. Adv. *Electr. Electron. Eng*. 22 (3) 250–259 https://doi.org/10.15598/aeee.v22i3.5526.

[13] Novak, D., Cermak, P. (2015). Fuzzy-based method of detecting the environment character for UAV optical stabilization. *Adv. Electr. Electron. Eng*. 13 (3) 255–261 https://doi.org/10.15598/aeee.v13i3.1299.

[14] Hung, T., Nguyen, Q., Minh, B., Nguyen, T., Nguyen, N. (2025). Multi power beacon empowered secure in IoT networks: Secrecy outage probability analysis. *Adv. Electr. Electron. Eng*. 23 (2) 91–97 https://doi.org/10.15598/aeee.v23i2.241112.

[15] Bhatnagar, M. R. (2013). On the capacity of decode and forward relaying over Rician fading channels. *IEEE Commun. Lett*. 17, 1100–1103.

[16] Pham, T. H. T., Nguyen, N. T. T., Nguyen, Q. S., Nguyen, T. H., Minh, B.V., Nguyen, Q. S., Tran, M. (2025). Performance Analysis in D2D Partial NOMAAssisted Backscatter Communication. *Advances in Electrical and Electronic Engineering* https://doi.org/10.15598/aeee.v23ix.250314.

[17] Hung, T. C., Minh, B. V., Nguyen T. N., Voznak M. (2025). Power beacon-assisted energy harvesting symbiotic radio networks: Outage performance. PLoS ONE 20(2): e0313981. https://doi.org/10.1371/journal.pone.0313981.

[18] Zwillinger, D., Moll, V., Gradshteyn, I., Ryzhik, I. (2015). Table of Integrals, Series, and Products, 8th edn. Zwillinger, D. (ed.). Academic Press, Boston.